promoting access to White Rose research papers

White Rose Research Online

Universities of Leeds, Sheffield and York
http://eprints.whiterose.ac.uk/

This is an author produced version of a paper published in **Journal of Applied Physics**.

White Rose Research Online URL for this paper:
http://eprints.whiterose.ac.uk/9040

Published paper
Basu, S., Fry, P.W., Gibs, M.R.J., Schrefl, T. Allwood, D.A (2009) *Control of the switching behavior of ferromagnetic nanowires using magnetostatic interactions*, Journal of Applied Physics, 105 (8), Art no.083901
http://dx.doi.org/10.1063/1.3098251

White Rose Research Online
eprints@whiterose.ac.uk

Control of the switching behavior of ferromagnetic nanowires using magnetostatic interactions

S. Basu [1], P. W. Fry [2], M. R. J. Gibbs [1], T. Schrefl [1], and D. A. Allwood [1*]

[1] Department of Engineering Materials, University of Sheffield, Sheffield S1 3JD, United Kingdom

[2] Centre for Nanoscience and Technology, University of Sheffield, Sheffield S3 7HQ, United Kingdom

* **D.Allwood@sheffield.ac.uk**

Abstract

Magnetostatic interactions between two end-to-end Permalloy ($Ni_{80}Fe_{20}$) nanowires have been studied as a function of their separation, end shape and width. The change in switching field increases as the wires become closer, with deviations from the switching field of an isolated wire of up to 40 % observed. The sign of the change depends upon the relative magnetization orientation of the two wires, with higher fields for parallel magnetization and lower fields for anti-parallel magnetization. Wire end shape has a strong influence with larger field variations being seen for flat-ended wires than wires with tapered ends. The micromagnetic modeling and experiments performed here were in good qualitative agreement. The experimental control of switching behaviour of one nanowire with another was also demonstrated using magnetostatic interactions.

Introduction

Patterned ferromagnetic nanostructures are an interesting subject of research due to their potential for use in several technological applications.[1-4] Controlling their dynamic properties is important to ensure the correct operation of the proposed devices and magnetostatic interactions offer one route to achieving this. Isolated nanoscale magnetic dots of sufficiently small dimensions have uniform magnetic dipoles[5] and when in a non-interacting array, each dot responds to an applied magnetic field individually.[5] However, stray field interactions that arise for small dot separations can change the magnetization reversal process to collective rotation.[6] Magnetostatic interactions can be used to propagate information along chains of dots[7] or perform logic operations[4] in magnetic quantum cellular automata (MQCA) networks. Magnetic dipolar coupling of head-to-head domain walls was studied in NiFe and Co nanoring arrays.[8] The stray field intensity of the domain walls varied as the inverse of distance and at the smallest separations the spin structure of the interacting domain walls changed from 'vortex' to 'transverse'.[8] The switching behaviour of Permalloy ($Ni_{80}Fe_{20}$) nanowires placed side-by-side in an array has also been explored.[9,10] It was observed that the mode of switching of the nanowires in the array was dependent on their thickness, with the crossover point occuring a thickness-to-width ratio of 0.5. When nanowires of two different widths were placed in an alternating array, the switching fields became dependent on the width difference, but the magnetization reversal was initiated by switching of the wider wire.[10] There is only one report of magnetostatically-interacting nanowires placed end-to-end.[11] This was limited to modeling of 1.47 μm × 180 nm × 50 nm Permalloy wires, in which high remanence was observed for nanowire pairs with separations of 10 and 50 nm.[11] It was also found that the magnetizations of the wires were aligned along the wire axis due to strong dipole coupling.

Despite the strong magnetostatic interaction, the coercivity of these wires surprisingly remained close to that of single isolated wires.

Here we have studied the magnetostatic interaction of two end-to-end Permalloy nanowires as a function of their separation, end shape and width. Systematic variation of these parameters in combination with an applied field is used to control the switching behavior of one nanowire with the other.

Experimental

Our micromagnetic simulations use a finite element/boundary element method to solve the Landau-Lifshitz-Gilbert equation.[12] The nanowires were divided into tetrahedral elements with a mesh size of 5 nm within 50-100nm of an interacting wire end and 10 or 20 nm elsewhere. The larger size of the mesh did not have any noticeable effect on the behavior of the nanowires. The wires were assigned the material properties of Permalloy (exchange constant=1.3×10^{-11} J/m, saturation magnetization=800 kA/m) while neglecting the magneto-crystalline anisotropy. The stray magnetic field emanating from the nanowires was calculated along the long axis of the nanowire with a step size of 10 nm. Figure 1 shows the nanowire geometries, the combination of nanowire end shapes, and the initial magnetizations employed for the study. The wire ends were either flat or one of two tapered geometries [Fig 1(b)], where the ratio P of the tapered section length to the nanowire width was either 0.87 or 1.73. One nanowire in the pair had a fixed width, w, of 200 nm while the w of the other nanowire had value of 100, 150 or 200 nm. The nanowire length was varied from 700 nm – 1.53 μm, excluding any tapering, but this did not affect the switching properties. The thickness of all modeled nanowires was 10 nm. In order to study the magnetization reversal at one end of a wire, the other end had to be more stable. This was achieved by ensuring the end of interest was less tapered than the other end.[13]

Wire separations, *D*, of 20 – 200 nm were investigated. After initializing the modeled structures under zero field, the magnetic field magnitude was increased at a rate of 1 Oe/ns in the parallel (+x) or anti-parallel (–x) direction until one or both the wires switched. Each wire pair was tested under both anti-parallel [Fig. 1(c), 1(e), 1(g)] and parallel [Fig. 1(d), 1(f), 1(h)] initial magnetization configurations. Flat-ended wires contained an end domain parallel to the wire end [Fig. 2(a)] to reduce the magnetostatic energy contribution whereas the tapered wire ends [Fig. 2(b)] did not. When two flat ended wires were initialized, the end domains were either parallel or antiparallel to each other.

Experimental nanowire structures were fabricated by electron beam lithography, thermal evaporation of 10 nm of Permalloy (plus a 2 nm Au capping layer) and ultrasonic lift-off in acetone. The wires were 20 μm long (without tapering at the end), 200 nm wide and 10 nm thick. Figure 3 shows a typical SEM micrograph of (a) tapered-flat (+pad) ended wires and (b) tapered-flat ended wire. The wires are seen to have considerable edge roughness but this does significantly affect the experiment since nucleation fields are measured rather than the more sensitive domain wall propagation fields. The tapering geometries used for the simulation were retained in the fabricated wires. The switching fields of the magneto-statically interacting nanowires were measured by magneto-optical Kerr effect (MOKE) magnetometry. The magnetometer[14] uses a 532 nm wavelength continuous wave laser at an angle of 45° to the sample focused to a 4 μm × 7 μm spot (FWHM). Hysteresis loops were obtained by applying ac magnetic fields at a frequency of 27 Hz to wires along their long (easy) axis using an electromagnet. The separation between nanowire pairs was measured by scanning electron microscopy (FEI Sirion Field Emission Gun scanning electron microscope).

To create the condition of anti-parallel magnetization in the wires, pads of 4 μm × 4 μm were attached to one of the nanowires in the pair [Fig. 3(b)]. These act as low field

domain wall sources[15,16] and allow the attached wire to be reversed at this field to achieve the anti-parallel magnetization configuration.

Result and Discussion

Micromagnetic modeling was used to determine the magnetization reversal behavior of isolated 200 nm wide wires with flat or tapered ends. Under an applied easy axis magnetic field, a reverse magnetic domain nucleates in a flat wire end at 249 Oe by rotation of the end domain [Fig. 4(a)-(c)]. The resulting domain wall travels to the other end of the wire, reversing its magnetization. Magnetization reversal in tapered wire ends (P=0.87) occurs at the higher field of 345 Oe. However, domain nucleation originates from within the volume of the wire end [Fig. 4(d) and (e)], in agreement with previous work[17,18]

Figure 5(a) and (b) show the switching field, H_{sw}, of wires as a function of separation between nanowire pairs with anti-parallel and parallel initial magnetization, respectively. The switching fields of isolated wires (H_{sw}^{0}) with flat or tapered ends are also shown as dotted and dashed lines. A positive magnetic field was applied, meaning that negative magnetization (from right to left in Fig. 5) is reversed during the modeling. For interacting wires with initially anti-parallel magnetization, H_{sw} decreases from that of the isolated wire as they become closer [Fig. 5(a)]. Here, the anti-parallel magnetic configuration in the wires gives rise to opposing stray fields from the wire ends that assist in switching the opposite wire. With increasing separation, the effect of this stray field decreases. With parallel magnetization in the wires, the stray field interaction between the wires stabilizes the configuration and the switching field increases as the wire separation decreases [Fig 5(b)]. This general trend is not completely followed in the interaction of flat and taper-ended wires with initially parallel magnetization [Fig. 5(b)] since the flat-ended wire switches first, creating an anti-parallel magnetization configuration for the tapered

wire to switch from. Thus, H_{sw} for the flat-ended wire increases due to the magneto-static interaction but H_{sw} for the tapered wire always decreases.

It is noticeable from Fig. 5(a) for anti-parallel magnetization configuration that the interactions between flat-ended wires are much stronger than those between tapered wires. For example, H_{sw} for flat-ended wires can differ from H_{sw}^{0} by over 40 % at the closest separations whereas tapered wires achieve only a 5 % change at best. Furthermore, the flat-ended wire in the mixed pair shows a similar reduction in H_{sw} to the tapered wire pair. The situation becomes more complicated for the parallel initial configuration [Fig. 5(b)] since H_{sw} for flat-ended wire pairs depends critically on the relative alignment of the wire end domains. When these are parallel, the interaction is particularly strong and large increases in H_{sw} are predicted. When the end domains are anti-parallel, there is little change in H_{sw} across the range of separations used. This is surprising given that the anti-parallel end domain configuration has a lower total energy at remanence and, hence, would be expected to be more stable. The overall energy of the system is the resultant of the exchange, magneto-static and Zeeman energies. There is no difference in Zeeman energy between the anti-parallel and parallel end domain cases since the same field is applied. Near the switching field, the exchange and magneto-static energies are higher for the parallel end domain geometry compared to the anti-parallel end domain, indicating a higher energy barrier to reversal, giving rise to this behavior.

To understand the magnetostatic interactions better, we calculated the stray easy axis field, H_x, from the flat end of a nanowire along a line following the wire easy axis and halfway through the wire height (Fig. 6). Very close to the wire end ($d \leq 30$ nm), H_x falls off as a function of $1/d^3$, indicating that this is a field from a magnetic dipole. At larger distances ($d \geq 85$ nm), H_x decreases as $1/d^2$, indicating that a monopole field source now dominates. This dipole field arises from the poles of the end domains in the nanowires at

shorter distance, whereas, at a larger distance the field encountered is dominated by the easy axis domain in the wire. The inset in Fig. 6 shows the calculated field from a 100 nm wide wire. The stray field magnitude is higher close to the wire ($d \leq 30$ nm) compared to the 200 nm wide wire due to the end domain being energetically less favourable in the 100 nm wide wire. However, the field decreases more rapidly above $d = 40$ nm for the 100 nm wide wire due to it being narrower than the 200 nm wide wire.

The unequal width wire pairs had nanowires with either $w = 100$ and 200 nm or $w = 150$ and 200 nm. Here, the interacting ends were flat while the other ends were tapered ($P = 0.87$). The initialized wires had anti-parallel and parallel magnetization configurations with combinations of anti-parallel and parallel end domain magnetizations. When the wires had anti-parallel magnetization, both positive and negative fields were simulated to test the switching of both wires.

The calculated switching fields for interacting wide and narrow wires from initially anti-parallel magnetization between the wires is shown in Fig. 7(a) and (b), for parallel and anti-parallel end domains, respectively. The trends are similar to those found with the equal width wire pairs with antiparallel magnetization in the wires, with H_{sw} increasing with increasing wire separation. All of the narrower wires show approximately the same fractional change in H_{sw} of $\geq 35\%$. The larger switching fields of narrower wires means that these are subject to the largest absolute changes in H_{sw}, with changes of over 180 Oe for 20 nm separation compared with an isolated wire. The variation in H_{sw} for the 200 nm wide wires is slightly greater when paired with the 150 nm wide wire compared with the 100 nm wide wire, showing the greater strength of interaction from the wider wire. Changes in the relative orientation of the wire pairs' end domain magnetization doesn't appear to influence H_{sw} very strongly [Fig. 7(a) and (b)], as was seen for the anti-parallel wire magnetization configuration with wires of equal width.

With parallel initial magnetization and either parallel [Fig. 7(c)] or anti-parallel [Fig. 7(d)] end domains, there is a change in the dependence of H_{sw} on wire separation for the 150 and 200 nm wide wires. The lower value of H_{sw} for the 200 nm wide wires means that they invariably switch first, but now, H_{sw} for these widest wires increase with closer wire separations as the narrower wire has an increasingly stabilizing influence. Once the 200 nm wide wire magnetization is reversed, the wire pair enters the anti-parallel configuration and H_{sw} for the narrower wire is reduced from the isolated wire case. For the 100 nm wide wire, H_{sw} are identical for the equivalent separations shown in Fig. 7(a) and (b). For the narrowest separations considered with the 150 nm/200 nm wire pair, as soon as the 200 nm wide wire switches, the interaction between the wires is so strong that the 150 nm wire magnetization also reverses. Due to the large differences in H_{sw}^{0} between the wires in each pair, the relative initial orientation of the end domains is of little consequence, unlike the situation with a pair of 200 nm wide wires [Fig. 5(b)].

Experimentally determined switching fields from interacting nanowire pairs are shown in Fig. 8.When one of the wires had a domain wall injection pad attached the wire switched at a low field (~ 95 Oe) allowing us to measure the switching field of the other wire using an anti-parallel wire magnetization configuration [Fig. 8(a)]. The absolute values of measured switching fields are much lower than those given by the modeling above, as can be expected for room temperature experiments compared with simulations of systems at 0 K. However, the experimental data reflect the trend of increased switching field with increased separation for wires with opposite magnetization that is predicted by modeling. As was seen in the modeling, flat-ended wires showed a larger deviation from H_{sw}^{0} than tapered wires, with a change of ~ 13 % for a 50 nm wire separation. This compares to a modeled change of ~ 15 and 19 % for parallel and anti-parallel end domains for the same separation. We were unable to fabricate wires with separations narrower than

50 nm in order to test the strongest interactions. Wire pairs without pads were used to test the initially parallel magnetization configuration [Fig. 8(b)]. This arrangement stabilizes the magnetization of the wires so that the flat-ended wires did not switch until fields higher than H_{sw}^{0} are reached. At 60 nm separation, the maximum change in switching field is ~ 13 %, very close to that observed with 50 nm separation in Fig. 8(a). The pointed wire in a pointed-flat pair shows very little change, as seen in modeling [Fig. 5(b)]. More surprising was the observed reduction in switching field for the pointed wire pair. We believe this is due to edge roughness in the fabricated wire ends, leading to a change in the switching mechanism from volume nucleation to edge nucleation. This is also reinforced by the fact that the fractional change in switching field for the tapered wire in 8 % whereas the modeled changed is less than 2 %.

The switching property of one nanowire can be controlled with another. To demonstrate this, we measured a nanowire pair consisting of a tapered wire and flat ended wire pair without injection pad with D = 102 nm. The MOKE laser spot was positioned to be sensitive to both wires simultaneously. The hysteresis loop obtained under a high magnetic field amplitude H = 369 Oe [Fig. 9(a)] showed magnetic transitions at 153 and 203 Oe. Additional MOKE measurements with the laser spot moved to the separate wires confirmed that these fields correspond to switching of the flat-ended and tapered wires, respectively. Clearly, for this measurement the wires have parallel initial magnetization. Now an intermediate field of H = 164 Oe was applied. The hysteresis loop becomes asymmetric with two different transitions of +152 Oe and – 109 Oe [Fig. 9(b)]. The higher switching field corresponds to one of the previous observed transitions and is consistent with the flat-ended wire reversing from a parallel magnetization state [Fig. 5(b) and Fig. 8(b)]. However, the ±164 Oe applied field is not sufficient to switch the tapered wire, so an antiparallel magnetization state is created in the wires. In the negative-going part of the

hysteresis loop, the lower field flat ended wire switching from the antiparallel magnetization configuration, confirming the magnetostatic interactions described above [Fig. 5(a) and Fig 8(a)]. At a lower applied field of ±136 Oe, no magnetic transitions was observed, as the flat ended wire did not switch from the parallel magnetization configuration in the wire pair at this low field [Fig. 9(c)]. This demonstrates how setting the magnetization of one wire (tapered ended) can be used to control the magnetization of the other. By application of a particular field for a particular geometry of wire pair, the switching of one wire with another can be controlled. At a higher separation of D = 178 nm, the magnetic transitions of the flat ended wire underwent magnetization reversal under an intermediate field at 143 Oe and 125 Oe. This indicates that changing the wire separation allows the dynamic range of the switching field variation to be controlled.

Conclusion

We have studied the magnetostatic interaction of two end-to-end Permalloy nanowires as a function of their separation, width and end shape by micromagnetic modeling and experiment. The interaction stabilizes parallel magnetization configurations between the wires but lowers the switching field of anti-parallel magnetization arrangements. The interactions become stronger as the wire separation reduces and for flat-ended wires rather than wires with tapered ends. Our limitations in fabrication have meant that the closest modeled separations of 20 nm have not been tested experimentally, although this separation might be achieved using a focused ion beam to cut a continuous wire or by e-beam techniques and an electron-transparent substrate. Magnetostatic-induced variations in the wire switching field of over 40 % of that of isolated wires are predicted. When wires of different widths are used, the narrower wire experiences significantly larger changes in switching field. This principle was used to demonstrate that the switching

properties of one nanowire can be controlled by another. As well as the possibility of controlling the reversal of one wire with another, this work could be helpful in understanding how closely spaced nanowires in an in-plane sensor arrangement[19] affect each other. Magnetostatic interactions between domains in thin films[20] previously had an impact of the development of all-magnetic logic, and the interactions observed here may also prove useful in biasing nanowire junctions[1]for logic operations.

Acknowledgement

The authors gratefully acknowledge EPSRC for financial support.

References

[1] D. A. Allwood, G. Xiong, C. C. Faulkner, D. Atkinson, D. Petit, and R. P. Cowburn, Science **309,** 1688 (2005).

[2] S. S. P. Parkin, M. Hayashi, and L. Thomas, Science **320,** 190 (2008).

[3] P. Xu, K. Xia, C. Gu, L. Tang, H. Yang, and J. Li, Nature Nanotechnology **3,** 97 (2008).

[4] A. Imre, G. Csaba, L. Ji, A. Orlov, G. H. Bernstein, and W. Porod, Science **311,** 205 (2006).

[5] R. P. Cowburn, D. K. Koltsov, A. O. Adeyeye, M. E. Welland, and D. M. Tricker, Phys. Rev. Lett. **83,** 1042-1045 (1999).

[6] L. J. Heyderman, H. H. Solak, C. David, D. Atkinson, R. P. Cowburn, and F. Nolting, Appl. Phys. Lett. **85,** 4989 (2004).

[7] R. P. Cowburn and M. E. Welland, Science **287,** 1466-1468 (2000).

[8] M. Laufenberg, D. Bedau, M. Kläui, U. Rüdiger, D. Backes, L. J. Heyderman, F. Nolting, C. A. F. Vaz, J. A. C. Bland, T. Kasama, R. E. Dunin-Borkowski, S. Cherifi, A. Locatelli, and S. Heun, Appl. Phys. Lett. **88,** 212510 (2006).

[9] S. Goolaup, N. Singh, A. O. Adeyeye, V. Ng, and M. B. A. Jalil, Eur. Phys. J. B **44,** 259 (2005).

[10] S. Goolaup, A. O. Adeyeye, N. Singh, and G. Gubbiotti, Phys. Rev. B **75,** 144430 (2007).

[11] W. Chen, D. R. Fredkin, and T. R. Koehler, IEEE Trans. Magn. **28,** 3186 (1992).

[12] D. Suess, V. Tsiantos, T. Schrefl, J. Fidler, W. Scholz, H. Forster, R. Dittrich, and J. Miles, J. Magn. Magn. Mater. **248,** 2981 (2002).

[13] K. J. Kirk, J. N. Chapman, and C. D. W. Wilkinson, J. Appl. Phys. **85,** 5237 (1999).

[14] D. A. Allwood, G. Xiong, M. D. Cooke, and R. P. Cowburn, J. Phys. D **36,** 2175 (2003).

[15] K. Shigeto, T. Shinjo, and T. Ono, Appl. Phys. Lett. **75,** 2815 (1999).

[16] R. P. Cowburn, D. A. Allwood, G. Xiong, and M. D. Cooke, J. Appl. Phys. **91,** 6949 (2002).

[17] X. F. Han, M. Grimsditch, J. Meersschaut, A. Hoffmann, Y. Ji, J. Sort, J. Nogués, R. Divan, J. E. Pearson, and D. J. Keavney, Phys. Rev. Lett. **98,** 147202 (2007).

[18] W. C. Uhlig and J. Shi, Appl. Phys. Lett. **84,** 759 (2004).

[19] N. Tombros, S. Tanabe, A. Veligura, C. Jozsa, M. Popinciuc, H. T. Jonkman, and B. J. van Wees, Phys. Rev. Lett. **101,** 046601 (2008).

[20] R. J. Spain, J. Appl. Phys. **37,** 2572 (1966).

Figure captions

Figure 1. Geometry of (a) nanowires and (b) tapered wire end for length *L*, width *w* and taper length s. (c)–(h) Scheme of combination of nanowire end shapes and initial magnetizations (indicated by arrows).

Figure 2. Initialized state of (a) isolated flat and (b) isolated taper-ended 200 nm wide wires. The circled areas are shown in Figure 3.

Figure 3. Micrograph of patterned magneto-statically interacting nanowires. (a) Tapered-flat wire pair (with pad) and (b) tapered-flat wire pair.

Figure 4. Time evolution of domain nucleation close to wires ends for (c)-(e) a flat-ended wire and (f)-(g) for a tapered wire. The arrows and color scheme represent a local average of magnetization. The directions of *x* and *y* are also indicated for use in the text.

Figure 5. Switching field magnitude of nanowire pairs as a function of their separation for (a) antiparallel initial magnetization and (b) parallel initial magnetization. The symbols in the inset are adjacent to the wire type they represent. Also shown are the switching fields of isolated tapered (- - - -) and flat-ended (− · − · −) wires.

Figure 6. Calculated stray magnetic field H_x as a function of distance from the flat end of a 200 nm wide nanowire as a function of distance from the nanowire. The dotted line (yellow) and the dashed line (brown) are cubic and quadratic fits to the data. The inset shows the stray field profile for a 100 nm wide wire.

Figure 7. Switching field magnitude of unequal width flat-ended nanowire pairs as a function of their separation for (a) & (b) antiparallel initial magnetization with parallel and antiparallel end domain and (c) & (d) parallel initial magnetization with parallel and antiparallel end domain. The symbols in the inset are adjacent to the wire width they represent. Also shown are the switching fields of isolated 100 nm (·····), 150 nm (- - - -) and 200 nm (− · − · −) wide wires.

Figure 8. Measured switching field magnitude of 200 nm wide nanowire pairs as a function of their separation (a) for wires adjacent to a wire having a pad (antiparallel initial magnetization) (b) for wires in a pair with no pad (parallel initial magnetization). The horizontal error bars are the range of separation between the wires for each data point. The vertical error bars represent standard error in the switching fields. The symbols in the inset are adjacent to the wire type they represent. Also shown are the switching fields of isolated tapered (- - - -) and flat-ended (− · − · −) wires.

Figure 9. (a) H_x = 369 Oe, both flat and tapered ended wires switched. (b) H_x = 164 Oe, only flat ended wire switched and the switching field depended on the initial magnetization configuration in the wires (c) H_x = 136 Oe, field too low to switch any wire.

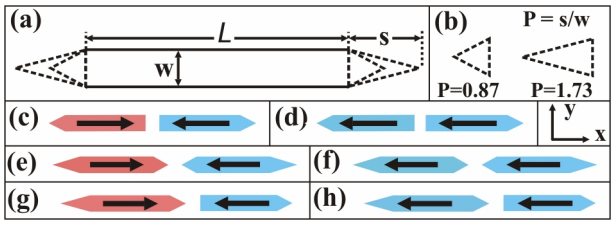

Figure 1

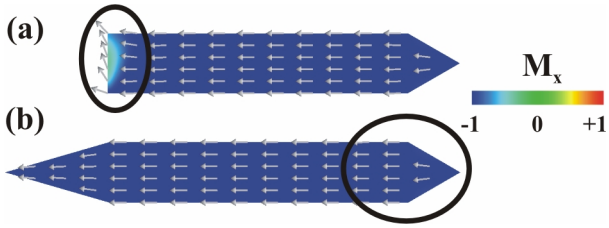

Figure 2

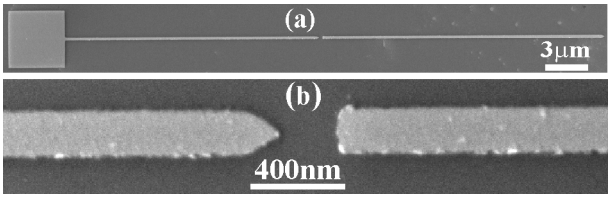

Figure 3

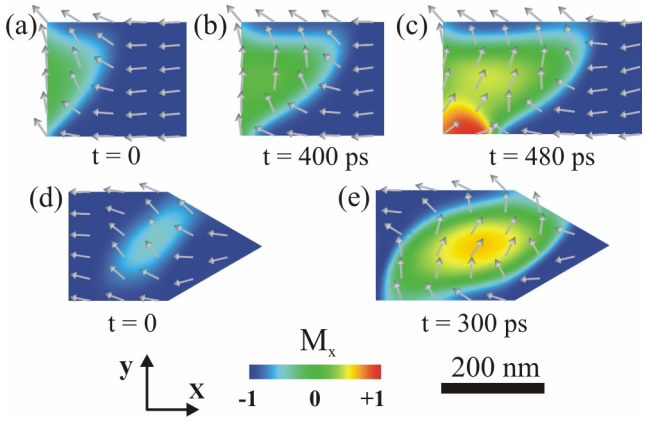

Figure 4

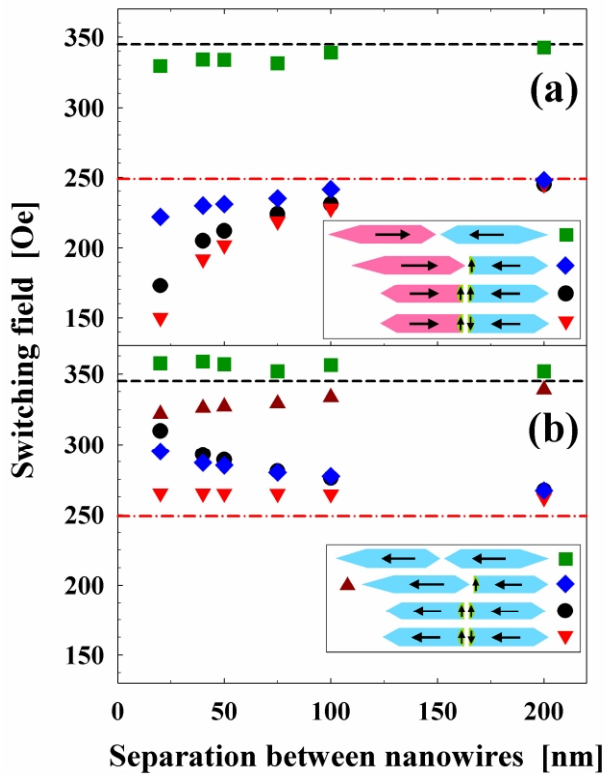
(a)
(b)
Switching field [Oe]
Separation between nanowires [nm]
350
300
250
200
150
0
50
100
150
200

Figure 5

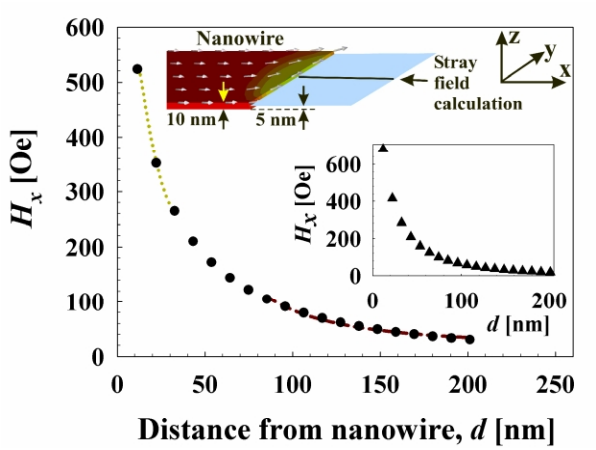
Nanowire
Stray field calculation
z
y
x
10 nm
5 nm
H_x [Oe]
600
500
400
300
200
100
0
0
50
100
150
200
250
Distance from nanowire, d [nm]
H_x [Oe]
600
400
200
0
0
100
200
d [nm]

Figure 6

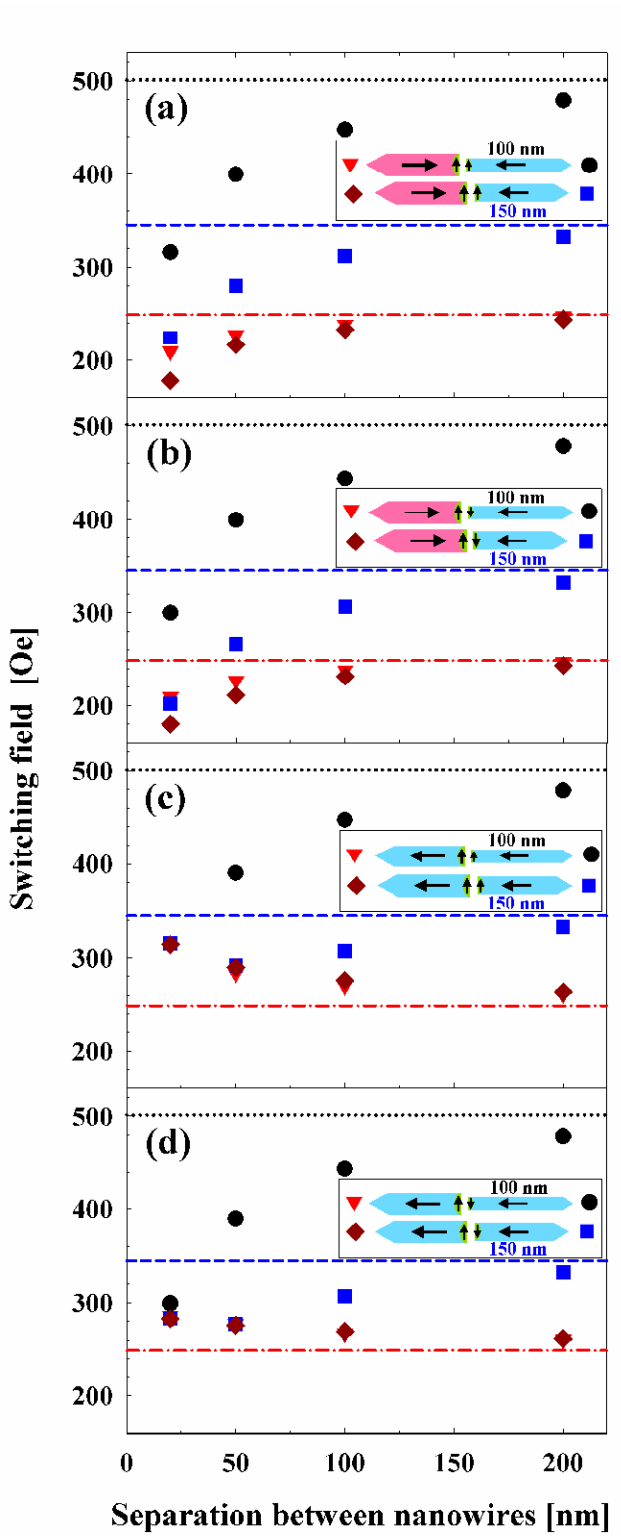
(a)
(b)
(c)
(d)
100 nm
150 nm
Switching field [Oe]
Separation between nanowires [nm]
500
400
300
200
0
50
100
150
200

Figure 7

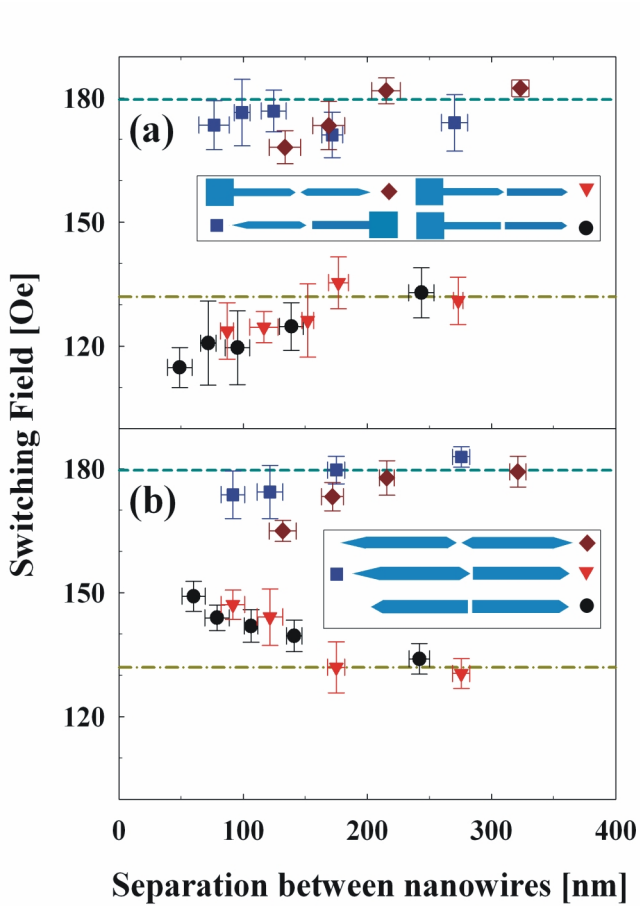
(a)
(b)
180
150
120
180
150
120
Switching Field [Oe]
0
100
200
300
400
Separation between nanowires [nm]

Figure 8

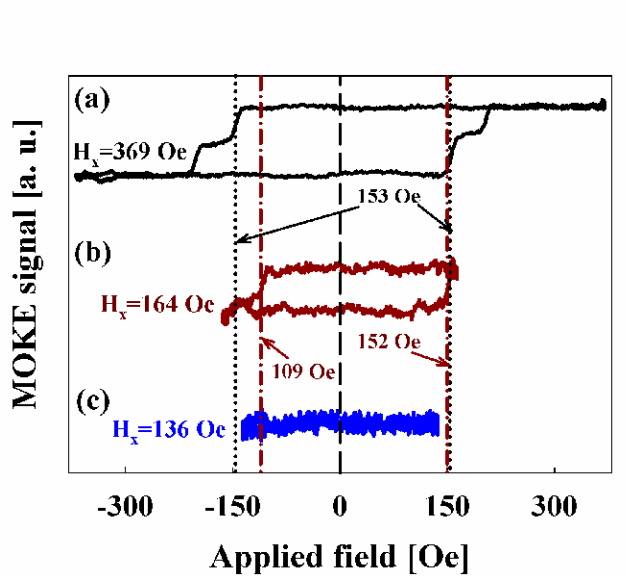
(a)
H_x=369 Oe
153 Oe
(b)
H_x=164 Oe
152 Oe
109 Oe
(c)
H_x=136 Oe
MOKE signal [a. u.]
-300
-150
0
150
300
Applied field [Oe]

Figure 9